Environmental Toxicology and Pharmacology 126 (2026) 105099

Contents lists available at ScienceDirect

Environmental Toxicology and Pharmacology

journal homepage: www.elsevier.com/locate/etap

"Testicular concentrations of metals and metalloids in dogs from the 'Land of Fires' (Campania Region, Italy): A preliminary morphological, chemical and molecular study"

Lorenzo Riccio [a,*], Maria De Falco [b,*], Marco Trifuoggi [c], Claudia Cucolo [b], Flavia Conte [d], Teresa Chianese [b], Nicola Ambrosio [e], Angelo Spada [e], Evaristo Di Napoli [a], Orlando Paciello [a,1], Luigi Rosati [b,1]

[a] Department of Veterinary Medicine and Animal Productions, University of Naples Federico II, Via Federico Delpino, 1, Naples, NA 80137, Italy
[b] Department of Biology, University of Naples Federico II, Via Vicinale Cupa Cintia, 21, Naples, NA 80126, Italy
[c] Department of Chemical Sciences, University of Naples Federico II, Strada Comunale Cinthia, 26, Naples, NA 80126, Italy
[d] Scuola Superiore Meridionale (SSM), Largo S. Marcellino, 10, Naples, NA 80134, Italy
[e] ASL Napoli 2 Nord DS 45 Caivano, Via S. Chiara, Caivano, Naples, NA 80023, Italy

ARTICLE INFO

Keywords:
One Health
Sentinel species
Reproductive toxicology
Testicular pathology
ICP-MS

ABSTRACT

In Campania Region, an area known as the '*Land of Fires*', has been described as an open-air dump due to the illegal discharges of toxic substances. The dog (*Canis familiaris*) represents a useful sentinel for tracking environmental risks. To this aim, fifty male stray dogs were enrolled, and testicular samples were processed for histological, chemical and molecular analyses. The animals were classified into four groups, from normal spermatogenesis to intratubular seminoma. Inductively coupled plasma mass spectrometry (ICP-MS) was conducted to assess metal and metalloid concentrations. Collagen deposition was assessed by Masson's trichrome and Picrosirius red staining. Immunohistochemistry and Western blot analyses were carried out to evaluate 17β-hydroxysteroid dehydrogenase (17β-HSD), Cytochrome P450 aromatase (P450), and the Proliferating Cell Nuclear Antigen (PCNA). Chemical analysis revealed significant group differences for cadmium, nickel and uranium levels across all histological groups. These findings suggest a distinct testicular profile, with differential metal accumulation by lesion severity and altered steroidogenic and proliferative processes.

1. Introduction

Human driven pollution has influenced the environment during the past fifty years, affecting ecosystems and the health of living organisms (Fuller et al., 2022; Prüss-Üstün et al., 2016). In the last decades, male infertility has increasingly been associated with exposure to environmental pollutants such as metals and metalloids. Among these elements, Cadmium (Cd), Nickel (Ni), and Uranium (U) have been associated with reduced male fertility and male reproductive dysfunction even at very low concentrations (Grison et al., 2022; Legendre et al., 2025; Lovaković, 2020; Parveen et al., 2024; Zhu et al., 2020). These substances are of particular concern for human and animal health, as they may impair testicular enzyme expression and the functions of Sertoli and Leydig cells (Mukherjee et al., 2022; Sharpe, 2024; Vinnikov and Syurin, 2024; Zhu et al., 2020). Nevertheless, the biological mechanisms linking exposure to metals and metalloids to canine testicular diseases remain unclear and require further investigation. Given the ubiquitous presence of these substances and their reproductive toxicity in both humans and animals, specific investigations in polluted areas are necessary to better understand the effects of these elements on animal reproductive health (Afzal and Mahreen, 2024; Esposito et al., 2019). In light of these observations, our study was developed in one of the most critical environmental contexts in Italy: '*The Land of Fires*', an area in Campania Region known for its illegal waste disposal including metals and metalloids (Alberti, 2022; Comba et al., 2006; Triassi et al., 2015). Although most studies have focused on mapping soil and water contamination risk or environment–cancer epidemiological studies (Alberti, 2022; Di Napoli et al., 2025; Ferrante et al., 2020; Triassi et al., 2015), to the best

* Corresponding authors.
E-mail addresses: lorenzo.riccio@unina.it (L. Riccio), madefalco@unina.it (M. De Falco).
[1] Co-last authors

https://doi.org/10.1016/j.etap.2026.105099
Received 27 March 2026; Received in revised form 21 June 2026; Accepted 14 July 2026
Available online 15 July 2026

of our knowledge, specific investigations addressing testicular accumulation of metals and metalloids in testicular tissue of dogs living in highly polluted areas in Campania Region are still lacking. From a One Health perspective, domestic dog (*Canis familiaris*) represents an excellent sentinel species for human environmental risks (Chen et al., 2023; Hampton et al., 2023; Ottaiano et al., 2025; Sumner et al., 2020). Indeed, humans and dogs share the same environment, resulting in exposure to the same contaminants. However, their shorter life expectancy also allows for earlier detection of the effects of chronic exposure, thus making them an ideal model system for investigating the effects of pollutants on the reproductive system (Pocar et al., 2023; Sumner et al., 2021). However, testicular toxicity may extend beyond germ cells depletion to include steroidogenic dysregulation, altered proliferative activity, and stromal remodelling. Consequently, an integrated approach is needed to characterize the biological mechanisms underlying testicular damage. In this context, 17β-hydroxysteroid dehydrogenase (17β-HSD) is a key marker of steroidogenic function and androgen biosynthesis, whereas cytochrome P450 aromatase (P450) informs on local estrogen pathway regulation and steroidogenic imbalance (Christin-Maitre and Young, 2022; Carreau and Hess, 2010; O'Donnell et al., 2001). The Proliferating cell nuclear antigen (PCNA) provides an index of proliferative activity and spermatogenic turnover (Sumner et al., 2021), while collagen deposition and changes in collagen fibre birefringence under polarised light reflect fibrotic remodelling of collagen and chronic tissue injury (Verderame et al., 2022; Rosati et al., 2023). Therefore, the aims of our study were to quantify testicular concentrations of metals and metalloids in dogs living in highly polluted areas and to investigate their association with histological, and molecular alterations in canine testes.

2. Materials and Methods

2.1. Ethics statement

All procedures were conducted in accordance with the European Directive 2010/63/EU and approved by the Ethical Animal Care and Use Committee of the University of Naples Federico II (Protocol No. PG/2023/0029409). Sampling was performed exclusively during routine castration procedures; no animal was sacrificed for research purposes or previously used in any clinical trials or treatments.

2.2. Area of sampling and inclusion criteria

Canine testes (total number 100) were obtained from 50 stray mixed-breed dogs after routine castrations performed at the Health District of Caivano (ASL Napoli 2 Nord DS 45 Caivano) between March 2023 and March 2025. All dogs included in the study originated from municipalities within the provinces of Naples and Caserta (details in Table 1). Inclusion criteria for the study were as follows: 1) dogs originating from the provinces of Naples and Caserta, within an approximate 40-km radius; 2) estimated age between 1 and 5 years, evaluated by a veterinarian; 3) adult male stray mixed-breed dogs of medium body size; 4) no administration of drugs or hormonal treatments known to affect spermatogenesis prior to orchidectomy. Immediately after surgery, ten micro-biopsies (~0.3 g each) were collected from each testis (total ~3 g per testis) and stored at −80 °C until use for chemical and molecular investigations. The remaining tissue was fixed and processed for histopathological analysis.

2.3. Histopathological analysis

2.3.1. Tissue processing, staining and image acquisition

Testes were cut following a longitudinal section plan and immediately fixed in 10% neutral buffered formalin (05–01005Q, BioOptica, Milan, Italy) for 72 h. After fixation, sections were trimmed, placed into the cassette, dehydrated, and embedded in paraffin wax. 3–4 μm sections were stained with Haematoxylin and Eosin (H&E) for basic morphology (Piegari et al., 2024), Masson's Trichrome (MT) (Zappulli et al., 2026) to assess collagen deposition, and Picrosirius-Red (PR) staining to assess collagen fibre birefringence (Power et al., 2026). Each stained cross-section was digitized and scanned with slide scanner (PANNORAMIC® 1000 DX, 3DHISTECH Ltd., Budapest, Hungary) and a free-access slide viewing software from the same firm, CaseViewer, was used (CaseViewer 2.3.0.99276, 3DHISTECH Ltd., Budapest, Hungary) to allow visualization and evaluation of the whole testis cross section (d'Aquino et al., 2026). Randomized pictures (fourteen images per testis) were taken on 10 × magnification and each picture represented at least 6–8 whole seminiferous tubules.

Table 1
Municipalities of origin of the enrolled dogs from the Provinces of Naples and Caserta. The left section lists municipalities from the Province of Naples, while the right section lists those from the Province of Caserta.

Geographic Area (Naples)	Age	Geographic Area (Caserta)	Age
Acerra (Na)	1 year	Caserta	1 year
Acerra (Na)	2 years	Caserta	3 years
Caivano (Na)	1 year	Caserta	2 years
Caivano (Na)	1 year	Caserta	4 years
Caivano (Na)	2 years	Caserta	5 years
Caivano (Na)	3 years	Francolise (Ce)	1 year
Casavatore (Na)	3 years	Francolise (Ce)	1 year
Casoria (Na)	3 years	Marcianise (Ce)	2 years
Frattaminore (Na)	1 year	Marcianise (Ce)	2 years
Frattaminore (Na)	2 years	Marcianise (Ce)	2 years
Giugliano (Na)	1 year	Mondragone (Ce)	1 year
Giugliano (Na)	3 years	Mondragone (Ce)	2 years
Giugliano (Na)	5 years	Mondragone (Ce)	2 years
Giugliano (Na)	2 years	Mondragone (Ce)	3 years
Marigliano (Na)	4 years	Orta di Atella (Ce)	1 year
Melito di Napoli	4 years	Orta di Atella (Ce)	3 years
Napoli	1 year	Pignataro Maggiore (Ce)	1 year
Napoli	1 year	Pignataro Maggiore (Ce)	1 year
Napoli	2 years	Riardo (Ce)	1 year
Napoli	3 years	Riardo (Ce)	2 years
Napoli	2 years	Ruviano (Ce)	1 year
Napoli	4 years	Ruviano (Ce)	1 year
San Giorgio a Cremano (Na)	4 years	Succivo (Ce)	2 years
Sant'Antimo (Na)	4 years	Succivo (Ce)	5 years
Sant'Antimo (Na)	2 years	Succivo (Ce)	3 years

2.3.2. Morphologic analysis and grading system

Histopathological assessment was carried out by two independent pathologists using a modified Johnsen scoring system (Johnsen, 1970). For each testis, 20 non-overlapping fields at high-power magnification (40 ×) were evaluated, and 100 seminiferous tubules were scored on a scale from 10 to 1 according to the presence or absence of spermatozoa, spermatids, spermatocytes, spermatogonia and Sertoli cells. The overall Johnsen score (JSC) for each testis was calculated as the mean of the scores of all evaluated tubules. In agreement with Sumner et al. (2021), which provided a baseline for defining abnormalities in canine testes, JSC values ≤ 7 were considered atypical. Each dog was assigned a single histological category based on the lesion found in most tubules observed in one of the testes, as follows:

Group A (normal spermatogenesis): dogs in which both testes showed normal spermatogenesis or only minimal disorganisation, corresponding to JSC 10–8.

Group B (mildly altered spermatogenesis): dogs with no neoplasia and at least one testis showing mild-to-moderate spermatogenic impairment (reduced spermatozoa and/or predominance of early germ cells), corresponding to JSC 7–4, while the contralateral testis ranged from normal to mildly affected.

Group C (severely altered spermatogenesis): dogs with no neoplasia and both testes exhibiting moderate-to-severe degeneration (germinal epithelium atrophy, Sertoli cell loss, spermatogenic arrest), corresponding to JSC 3–1.

Group D (neoplastic): dogs in which at least one testis displayed intratubular seminoma, irrespective of the condition of the contralateral testis.

2.4. Chemical analysis

Chemical analyses were conducted at the laboratory ACE-Analytical Chemistry for the Environment of the University of Naples Federico II. Sample and solution preparation were performed using deionised ultrapure water, which was acquired from a Milli-Q unit (Millipore, United States) with resistivity $\rho \geq 18.2$ MΩ·cm. Ultrapure nitric acid (HNO_3, 69% v/v, Ultratrace® grade for ppb-trace analysis) obtained from Scharlau (Barcelona, Spain) was used. The following multi-element solutions were used to construct the calibration curves needed for quantification and instrumental controls: IMS−120, Multielement Inductively Coupled Plasma Mass Spectrometry (ICP-MS) calibration standard 30 analytes, and IMS−108, Multielement ICP-MS calibration standard 21 analytes were obtained from Ultra Scientific Italia S.r.l. (Bologna, Italy); single-element solutions of Hg and Sn standard for ICP-MS 1000 mg/L were purchased by Sigma Aldrich (Merck KGaA, Darmstadt, Germany). Testicular tissue aliquots from the 50 recruited dogs, previously stored at −80 °C, were allowed to thaw completely at room temperature. Once thawed, approximately 0.5 g of tissue was weighed for each sample. Subsequently, 1 mL of ultrapure HNO_3 (69% v/v) was added to each aliquot. Tissue samples were digested using a closed-vessel microwave digestion system (Milestone ETHOS™ UP) equipped with PTFE (Teflon) vessels. Microwave-assisted acid digestion is widely recognized as an effective technique for sample preparation prior to ICP-MS analysis, as it ensures complete decomposition of the matrix under controlled high temperature and pressure conditions (Remeteiová et al., 2020). The digested samples were allowed to cool to room temperature and then diluted with deionised ultrapure water (whose resistivity is ≥ 18.2 MΩ·cm) to reach a final volume of 10 mL. Each sample was subjected to a single digestion procedure and then analyzed by ICP-MS. The instrument automatically performs three consecutive readings for each sample (technical triplicate), and the final concentration reported corresponds to the mean of these three instrumental measurements, calculated based on the calibration curve. Elemental concentrations were expressed on a wet-weight basis throughout the manuscript. The determination of metal concentrations in testicular tissue was carried out using an ICP-MS system (ICP-MS, iCAP RQplus, Thermo Fisher Scientific), operating in KED mode (Kinetic Energy Discrimination) (CASRN, 2007). Calibration standards were freshly prepared for each analytical session using certified single-elements and multi-elements stock solutions, diluted with nitric acid 2%, v/v. A total of 25 elements were quantified: As, B, Ba, Be, Cd, Co, Cr, Cu, Fe, Hg, Li, Mn, Mo, Ni, Pb, Rb, Sb, Se, Sn, Sr, Te, Tl, U, V, Zn. To ensure data accuracy and compensate for instrumental drift and matrix effects, ^{89}Y, $^{1\ 15}In$, ^{175}Lu and ^{103}Rh were employed as internal standards. Internal standard recoveries were monitored for each sample and were required to fall within the range of 80–120% to validate the corresponding results. For each analytical session, calibration curves were constructed over the concentration range 0.1–1000 μg/L, using at least five calibration points and verifying that the linear correlation coefficient (R^2) was ≥ 0.996. Quantification was performed using external calibration curves, which correlate the instrumental response (counts per second, cps) with the analyte concentration. For each element, calibration curves were built using multi-element standard solutions over an appropriate concentration range. Reagent and procedural blanks were included in each analytical batch and analyzed under the same conditions as the samples to monitor potential contamination. The concentrations of Ni, U, Sn, and V, as well as those of the other detected elements, were carefully evaluated to exclude potential contributions from blanks, carry-over, and contamination sources during both digestion and ICP-MS analysis. Carry-over (memory effects) was minimized through appropriate rinsing between samples using nitric acid solutions (HNO_3 2%, v/v), along with adequate wash times. Analytical reliability was ensured through method optimization and internal quality assurance and quality control (QA/QC) procedures. Different digestion mixtures ($HNO_3 + H_2O_2$, HNO_3 + HCl, and HNO_3 alone) were systematically evaluated in terms of recovery and potential interferences. Nitric acid alone was selected as it provided comparable recoveries while minimizing spectral interferences and ensuring a cleaner analytical background. The robustness of the method was further supported using blanks, internal standards, multi-point calibration, calibration verification standards, and instrumental triplicate measurements. These combined approaches support the reliability of the dataset.

2.5. Collagen deposition

The grade of collagen deposition was evaluated on Masson's trichrome-stained sections using ImageJ software (version 1.53 t). Ten randomly selected high-power fields (HPFs, 40 ×) were analysed per case. For each field, the area occupied by connective tissue was quantified by measuring the blue pixel area using the Colour Threshold function (HUE 150–190; Saturation 0–255; Brightness 0–180). The blue-stained area was measured as a percentage of the total field area. Subsequently, percentage values were converted into a semi-quantitative fibrosis score according to Damiano et al. (2023): score 0 (absent/physiological, <5% area); score 1 (mild, 5–10% area); score 2 (moderate, 10–30% area); and score 3 (severe, >30% area).

The final score for each case was obtained by averaging the scores recorded in the 10 HPFs for each testis and then calculating the mean value of the two testes; group data are expressed as mean ± standard error of the mean (SEM).

Polarised light observation of Picrosirius Red (PR) staining was used to assess collagen fibre organisation and birefringence patterns. Red/orange and green/yellow-green birefringence have traditionally been associated with differences in collagen fibre thickness, packing, and organisation (Junqueira et al., 1979; Lattouf et al., 2014). However, in the present study, birefringence patterns were treated as optical descriptors rather than as direct markers of collagen subtype or definitive maturation stage (Dayan et al., 1989; López De Padilla et al., 2021).

For each case, five randomly selected, non-overlapping fields were captured at 200 × magnification using a Zeiss Axioskop microscope equipped with a Zeiss Axiocam 305 colour camera and Zen Blue software (Verderame et al., 2022). Each image was decomposed into hue, saturation, and brightness (HSB) components using the Colour Threshold function in ImageJ® software (version 1.53 t). The hue component was retained, and a histogram of hue frequency was obtained from the resulting 8-bit hue images containing 256 colour values. Hue thresholds were defined as red/orange, 0–51, and green/yellow-green, 52–120 (Rosati et al., 2023), following established principles of Picrosirius Red analysis under polarised light (Junqueira et al., 1979; Lattouf et al., 2014). The areas occupied by red/orange and green/yellow-green birefringent pixels were quantified separately as percentages of the total tissue area. The resulting percentages were converted into semi-quantitative scores as follows: 0 = absent; 1 = low (<10%); 2 = moderate (10–30%); and 3 = high (>30%). For each case, the final red/orange and green/yellow-green birefringence scores were obtained by averaging the scores recorded in the five fields per testis and then calculating the mean value of the two testes; group data were expressed as mean ± SEM.

2.6. Immunohistochemical examination

Immunohistochemistry was performed using a well-established protocol (Agnese et al., 2014; Riccio et al., 2025) to investigate the testicular distribution of the following proteins: 17β-hydroxysteroid dehydrogenase (17β-HSD), Cytochrome P450 aromatase (P450), and Proliferating Cell Nuclear Antigen (PCNA). Briefly, 4 μm thick sections were mounted on poly-L-lysine slides (Menzel-Glaser, Braunschweig,

Germany). Endogenous peroxidase activity was inhibited using 3% hydrogen peroxide (H2O2) in methanol for 20 min. Antigen retrieval pretreatments were executed using a heat-induced epitope retrieval (HIER) 10 mM citrate buffer (pH 6.0) for 10 min at 92 °C. Then, slides were treated with a protein block (MACH1, Biocare Medical LLC, Concord, CA, USA) for 30 min each. Slides were incubated overnight at 4 °C with the primary antibodies diluted in phosphate-buffered saline (PBS) (0.01 M PBS, pH 7.2). The primary antibodies and dilutions used for this study are summarized in Table 2. After incubation with the primary antibodies, sections were incubated for 30 min at room temperature (for both mouse and rabbit antibodies) with an HRP-polymer detection system (MACH 1, Biocare Medical, Concord, CA, USA) according to the supplier's instructions. Finally, antibody reaction was visualized using the 3,3′-diaminobenzidine (DAB) chromogen diluted in the DAB substrate buffer; subsequently, the slides were counterstained with Carazzi's Haematoxylin. For the negative control sections, the primary antibody was either omitted or replaced with a 1:20 dilution of mouse serum for mouse monoclonal antibodies and normal rabbit serum for rabbit antibodies (Code 011–000–120, Jackson Immuno Research, West Grove, PA, USA) (d'Aquino et al., 2023). Slides were digitized and scanned with slide Scanner (PANNORAMIC® 1000 DX, 3DHISTECH Ltd., Budapest, Hungary) and a free-access slide viewing software from the same firm, CaseViewer, was used (CaseViewer 2.3.0.99276, 3DHISTECH Ltd., Budapest, Hungary) for descriptive evaluation. Cellular localization and staining pattern were assessed descriptively, while staining intensity and the distribution of immunopositive cells were evaluated semi-quantitatively by two independent observers blinded to the experimental groups, in accordance with previously described immunohistochemical scoring approaches (Bencze et al., 2021; Vaccaro et al., 2024). For each marker and case, ten randomly selected, non-overlapping fields were examined using a 40 × objective. A composite score integrating staining intensity and the distribution of immunopositive cells was assigned to each field as follows: 0 = absent, 1 = weak/focal, 2 = moderate/multifocal, and 3 = strong/diffuse (Bencze et al., 2021; Vaccaro et al., 2024). The final score for each case was calculated as the mean of the ten fields. Mean scores were converted into semi-quantitative categories as follows: − = absent (0), + = weak (>0–1.5), + + = moderate (>1.5–2.5), and + + + = strong (>2.5–3).

2.7. Western Blot analysis

Western blot analysis was performed to assess the relative protein expression levels of 17β-HSD, P450 aromatase, and PCNA. Frozen tissue samples were collected from eight dogs per group (total N = 32). For each animal, a single testicular sample was selected for western blot analysis according to the histopathological classification: normal testes in Group A, mildly altered testes in Group B, severely affected testes in Group C, and neoplastic testes in Group D. Tissue samples were homogenized in ice-cold radioimmunoprecipitation assay (RIPA) buffer with 1 × protease cocktail inhibitors. The suspension of homogenized tissues was centrifuged at 14,000 rpm for 10 min at 4 °C for protein extraction. The protein concentration of samples was measured using a Bradford assay (Bio-Rad Laboratories Inc., Hercules, CA, USA) (Chianese et al., 2024; Hmidi et al., 2026). Thirty micrograms of total protein extracts for each sample were boiled in Laemmli buffer for 5 min at 95 °C before sodium dodecyl sulfate–polyacrylamide gel electrophoresis (SDS–PAGE, 10% polyacrylamide). After electrophoresis, proteins were electro-transferred onto a nitrocellulose membrane. Each membrane was first blocked in 5% non-fat milk (in 25 mM Tris, pH 7.4; 200 mM NaCl; 0.5% Triton X-100, TBS/Tween) for 1 h at room temperature and then incubated overnight at 4 °C with one of the following primary antibodies: anti−17β-HSD, anti-P450 aromatase, and anti-PCNA. The primary antibodies and dilutions used for this study are summarized in Table 2. The following day, after three washes with TBS-Tween, membranes were incubated with the appropriate secondary antibodies (anti-rabbit IgG or anti-mouse IgG) conjugated with horseradish peroxidase (HRP) and diluted 1:1000 in 2.5% non-fat milk–TBS-Tween for 1 h at room temperature. After the last three washes with TBS-T, signal detection was performed using enhanced chemiluminescence (ECL) (Bio-Rad Laboratories Inc., Hercules, CA, USA), and the images were acquired using a ChemiDoc Molecular Imager (Bio-Rad Laboratories Inc., Hercules, CA, USA). The densitometric analysis was performed using ImageJ software (National Institutes of Health, Bethesda, Rockville, MD, USA) and normalized to GAPDH (Glyceraldehyde−3-phosphate dehydrogenase) to account for variations in loading.

Table 2
List of primary antibodies for immunohistochemical analysis, including host species, source, and working dilution.

Primary antibody	Host species	Source (Company, Location)	Dilution
17β-HSD (17β-hydroxysteroid dehydrogenase)	Mouse	Santa Cruz Biotechnology, Santa Cruz, CA, USA	1:300 (IHC); 1:800 (WB)
Aromatase (Cytochrome P450)	Rabbit	Santa Cruz Biotechnology, Santa Cruz, CA, USA	1:250 (IHC); 1:800 (WB)
PCNA (Proliferating Cell Nuclear Antigen)	Rabbit	Elabscience, Bionovation Inc., Rome, IT	1:400 (IHC); 1:900 (WB)
GAPDH (Glyceraldehyde−3-phosphate dehydrogenase)	Rabbit	Elabscience, Bionovation Inc., Rome, IT	1:1200 (WB)

2.8. Statistical analysis

Normality was assessed using the Shapiro–Wilk test. Dog age was compared between the Naples and Caserta subsets using a two-sided Mann–Whitney *U* test to assess geographic age imbalance. Because elemental concentrations and collagen scores were non-normally distributed, non-parametric tests were applied. For chemical analyses, the dog was considered the independent experimental unit. Elemental concentrations were primarily summarised as the mean of both testes per dog; sensitivity analyses were performed using one testis per dog, selected according to the highest histological severity category. Values below the limit of detection were imputed as LOD/2. P values were adjusted using the Benjamini–Hochberg procedure. Significant omnibus tests were followed by prespecified pairwise Mann–Whitney U tests comparing Group D with Groups A–C, with Holm–Šidák correction. Effect sizes were estimated using Cliff's delta. An exploratory heatmap based on log-transformed, z-standardised elemental concentrations was generated to visualise multi-element profiles across groups. Post-hoc comparisons for collagen scores were performed using Dunn's test. Western blot data were analysed by one-way ANOVA followed by Tukey's post-hoc test; two-sided p values < 0.05 were considered statistically significant.

3. Results

3.1. Age distribution

Dogs from the Province of Naples (n = 25) and the Province of Caserta (n = 25) showed comparable age distributions. Median age was 2 years in both groups (range, 1–5 years). No significant age difference was detected between dogs from the Naples and Caserta provinces ($p > 0.05$), indicating no marked age imbalance between the two geographic subsets (Fig. 1).

3.2. Morphologic evaluation

H&E sections from both testes of each dog were independently examined by two veterinary pathologists, and dogs were classified into

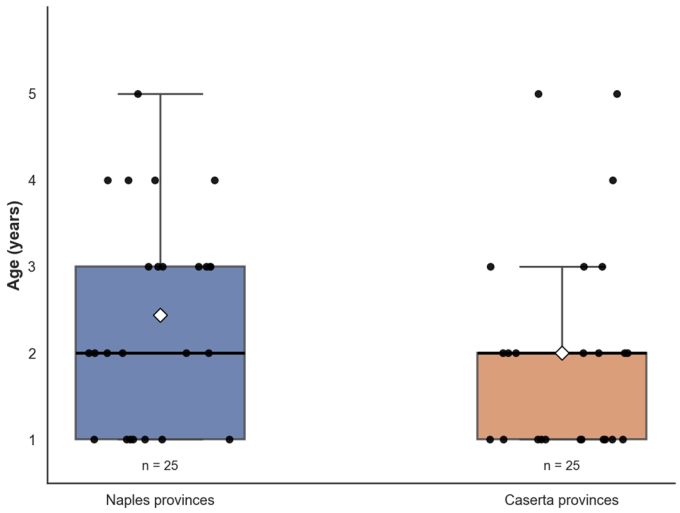

Fig. 1. Age distribution of dogs from the Province of Naples and Province of Caserta. No statistically significant difference was detected between the two geographic subsets ($p > 0.05$). Boxes represent the median and interquartile range, whiskers indicate the range, points represent individual dogs, and white diamonds indicate the mean.

four histological groups (A–D) based on the predominant morphologic pattern observed in either testis as follows:

Group A (n = 18 dogs; 36 testes): all dogs showed bilateral normal spermatogenesis with preserved testicular architecture (Fig. 2A). Seminiferous tubules exhibited complete germ cell maturation with minimal or no disorganisation. In detail, seminiferous tubules contained germ cells at all stages of differentiation, from spermatogonia at the basal compartment to luminal spermatozoa, in close association with Sertoli cells.

Group B (mildly altered, n = 10 dogs; 20 testes): in dogs belonging to this group, at least one testis showed mild-to-moderate spermatogenic impairment (Fig. 2B). Among the altered testes (11 out of 20), seven were completely devoid of spermatozoa, four contained only rare spermatids or predominantly early germ cells, while the contralateral testes (9 out of 20) displayed normal or near-normal morphology.

Group C (severely altered, n = 14 dogs; 28 testes): all dogs exhibited bilateral moderate-to-severe degenerative changes, including tubular atrophy, germ cell hypoplasia, Sertoli cell loss, germ cell vacuolisation, basement membrane thickening, and Leydig cell hyperplasia (Fig. 2C).

Group D (neoplastic, n = 8 dogs; 16 testes): at least one testis per dog displayed intratubular seminoma (8 neoplastic testes), characterised by sheets and nests of neoplastic germ cells replacing the normal tubular architecture (Fig. 2D). The contralateral testes (8 out of 16) ranged from mild to severe degenerative changes.

3.3. Chemical results

Concentrations of 25 elements were measured in both testes from each dog and analysed at the dog level, with the dog treated as the independent experimental unit. In the primary analysis, dog-level values were calculated as the mean of both testes for each animal across all groups, including Group D. To assess the robustness of tissue-selection strategy, a secondary lesion-oriented sensitivity analysis was performed using one testis per dog, selected according to the highest histological severity category; in Group D, this corresponded to the neoplastic testis. The dataset comprised 18 dogs in Group A (36%), 10 in Group B (20%), 14 in Group C (28%), and 8 in Group D (16%). Values below the analytical limit of detection were imputed as LOD/2 for statistical analyses. Inferential analyses were restricted to a primary panel of toxicological interest comprising As, Cd, Cu, Mo, Ni, Sn, U, and V, whereas all 25 quantified elements were retained for descriptive reporting. Descriptive statistics for all quantified elements by group are provided in Supplementary Material, Appendix A (Table S1).

Within the primary panel, Group D generally showed higher concentrations and greater variability than Groups A–C, particularly for Cd, Ni, and U (Fig. 3). In the primary dog-level bilateral analysis, Kruskal–Wallis tests with FDR correction identified significant overall group differences for Cd ($p < 0.05$), Ni ($p < 0.01$), Sn ($p < 0.05$), and U ($p < 0.001$), whereas As, Cu, Mo, and V were not significant after multiple-testing correction ($p > 0.05$). In the secondary sensitivity analysis, only Cd ($p < 0.05$), Ni ($p < 0.01$), and U ($p < 0.001$) remained significant after FDR correction, whereas Sn lost significance ($p > 0.05$). Thus, Cd, Ni, and U represented the most robust findings across tissue summarisation strategies. Full results of the overall group comparisons for both analytical strategies are reported in Supplementary Material, Appendix A (Table S2).

Post hoc Mann–Whitney U tests with Holm–Šidák correction were then performed for elements that remained significant after FDR correction, comparing Group D with Groups A–C. In the primary analysis, Cd differed significantly between Group D and Groups A, B, and C (all $p < 0.05$); Ni differed between Group D and Groups A, B, and C ($p < 0.001$, $p < 0.01$, and $p < 0.01$, respectively); Sn differed only between Group D and Group A ($p < 0.05$); and U differed between Group D and Groups A, B, and C (all $p < 0.01$). Consistent with the omnibus results, the secondary sensitivity analysis broadly confirmed the pattern observed in the primary analysis, supporting Cd, Ni, and U as the most consistent findings across tissue summarisation strategies. For the Group A versus Group D comparison in the primary analysis, Cliff's delta values were 0.65 for Cd, 0.80 for Ni, and 0.71 for U, indicating large effect sizes. Exploratory heatmap analysis of log-transformed and z-standardised concentrations showed a relative enrichment of higher multi-element burden profiles in Groups C and D (Fig. 4).

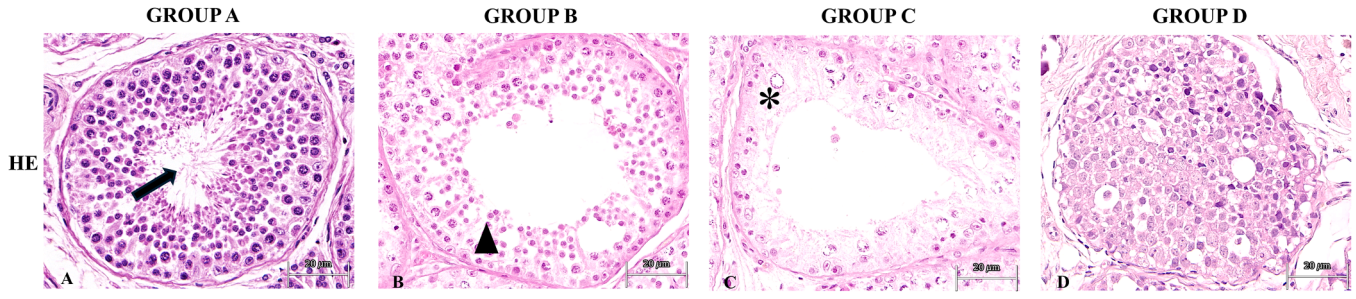

Fig. 2. Representative H&E-stained sections of canine testes from Groups A–D. (A) Group A shows normal testicular architecture with complete spermatogenesis and abundant luminal spermatozoa (black arrow). (B) Group B displays mild–moderate degeneration with partial loss of germ cells and reduced luminal spermatozoa (black arrowhead). (C) Group C shows severe degenerative changes with marked germ cell depletion and tubular atrophy (asterisk). (D) Group D presents intratubular seminoma, with sheets of neoplastic germ cells replacing the normal seminiferous tubular architecture. Original magnification: 60 × ; scale bar = 20 µm.

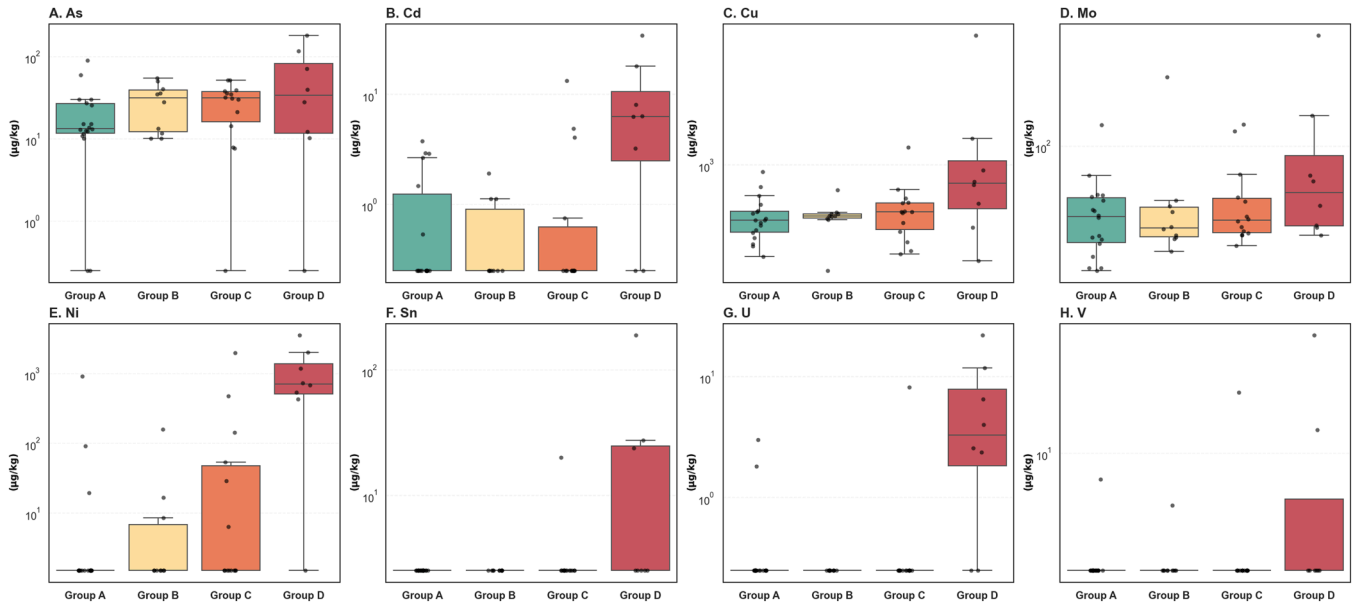

Fig. 3. Boxplots of log-scaled testicular concentrations of As, Cd, Cu, Mo, Ni, Sn, U and V across the four histological groups. Boxes represent the median and interquartile range, whiskers indicate 1.5 × the interquartile range, and points represent individual dogs.

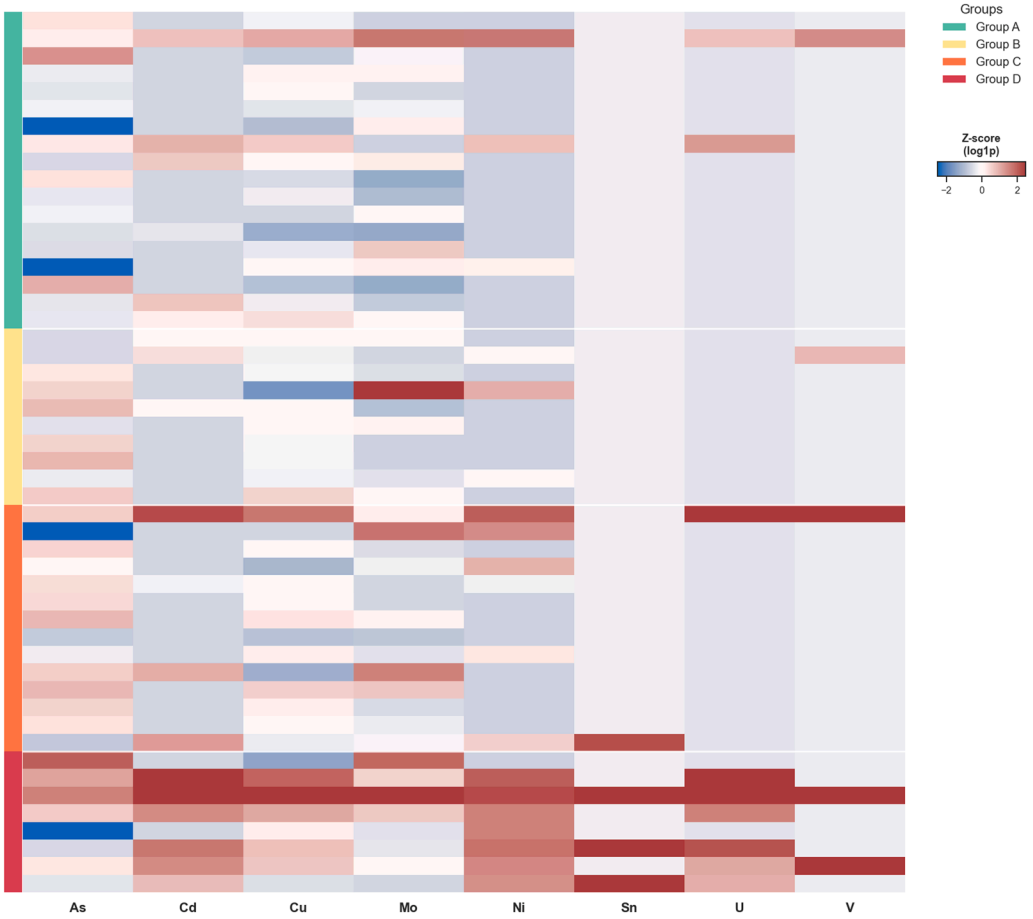

Fig. 4. Exploratory heatmap of log-transformed and z-standardised concentrations of As, Cd, Cu, Mo, Ni, Sn, U and V across the four histological groups. Each row represents one dog and each column one element; warmer colours indicate relatively higher values and cooler colours relatively lower values. Samples from Groups C and D tended to show relatively higher multi-element profiles.

3.4. Collagen deposition

Intratubular space alterations were quantified by assessing collagen content across the groups. Masson's trichrome staining revealed no excess collagen deposition in Group A testes (0.06 ± 0.02; Fig. 5A); whereas in Group B, collagen deposition scores were low but already increased compared with normal testes (0.83 ± 0.29; Fig. 5B, white arrow). Conditions of collagen hypersecretion and therefore of a potential fibrotic/inflammatory state increased in Group C (1.50 ± 0.50; Fig. 5C, white arrow) and reached the highest values in neoplastic testes from Group D (2.67 ± 0.29; Fig. 5D, white arrow), consistent with a progressive fibrotic remodelling from normal to severely altered and neoplastic tissue. After assessing the overall presence of collagen with Masson's trichrome staining, Picrosirius Red staining under polarised light was used to characterize the architectural features and spatial heterogeneity of collagen fibres (Fig. 5E–H).

In Group A, the peritubular compartment was characterized by thin fibres predominantly displaying green/yellow-green birefringence (1.67 ± 0.47; Fig. 5E, white asterisk). The inset illustrates an additional area from the same case in which scattered thick fibres with red/orange birefringence were also evident, highlighting heterogeneity in collagen fibre appearance.

Group B displayed a mixed architectural pattern, with thin green/yellow-green birefringent fibres (0.67 ± 0.29; Fig. 5F, white asterisk) and thick red/orange birefringent fibres (0.67 ± 0.29; Fig. 5F, white arrowhead). Compared with Group A, the green/yellow-green component was less represented, whereas the two birefringence patterns showed a more balanced distribution.

In Group C, the tissue architecture was markedly altered, with prominent thick red/orange birefringent fibres distributed within the interstitial compartment (0.83 ± 0.29; Fig. 5G, white arrowhead). The green/yellow-green birefringent component was also increased compared with Group B (1.17 ± 0.47). The inset shows an additional area from the same case in which thin green/yellow-green birefringent fibres were more clearly represented (Fig. 5G).

Neoplastic testes from Group D exhibited the most pronounced architectural alteration, characterized by extensive stromal networks of thick fibres showing marked red/orange birefringence (2.67 ± 0.29; Fig. 5H, white arrowhead). The green/yellow-green birefringent component also reached its highest value in this group (2.67 ± 0.29). The inset in Fig. 5H shows an adjacent peritumoural area in which thick red/orange bundles and thin green/yellow-green fibres occurred in close spatial proximity, highlighting the marked heterogeneity of stromal remodelling.

Kruskal–Wallis analysis followed by Dunn's post hoc tests revealed significant differences among groups in fibrosis severity and in both birefringent components. The semi-quantitative results are summarized in Fig. 6.

3.5. Immunohistochemical examination

In normal testes (Group A), 17β-HSD immunoreactivity showed a mixed nuclear and cytoplasmic distribution. Nuclear staining was evident in numerous germ cells within the seminiferous epithelium, whereas granular cytoplasmic immunoreactivity was observed in germ cells located in the basal compartment of the seminiferous tubules and in interstitial Leydig cells (Fig. 7A, black arrow and inset). In Group B, a comparable distribution pattern was observed, with clearly detectable nuclear staining and variable cytoplasmic immunoreactivity within the seminiferous and interstitial compartments (Fig. 7B). In testes showing degenerative alterations (Group C), 17β-HSD immunoreactivity was heterogeneous, discontinuous, and markedly reduced. Nuclear staining persisted in scattered residual germ cells, whereas cytoplasmic immunoreactivity was weak and focal in a limited number of germ cells and residual Leydig cells (Fig. 7C, black arrow and inset). In neoplastic testes (Group D), weak-to-moderate cytoplasmic staining was observed in tumour cells and in some interstitial elements, together with focal and variable nuclear staining (Fig. 7D, black arrow and inset). Overall, 17β-HSD showed a heterogeneous distribution comprising both nuclear and cytoplasmic components.

P450 aromatase immunoreactivity was primarily detected in the cytoplasm of Sertoli cells (Fig. 7E, black arrowhead) and in spermatozoa (Fig. 7E, white arrow) in normal testes. In Group B, staining became more diffuse within the seminiferous tubules and extended to the interstitial compartment (Fig. 7F, black and white arrowheads). In Group C, P450 aromatase immunoreactivity was more intense and widely distributed, with evident cytoplasmic labelling in Sertoli and interstitial cells (Fig. 7G, black and white arrowheads). In neoplastic testes (Group D), immunoreactivity was intense and diffuse in the cytoplasm of Sertoli-like and tumour cells (Fig. 7H, black arrowhead). Overall, the highest P450 aromatase immunoreactivity was observed in Groups C and D.

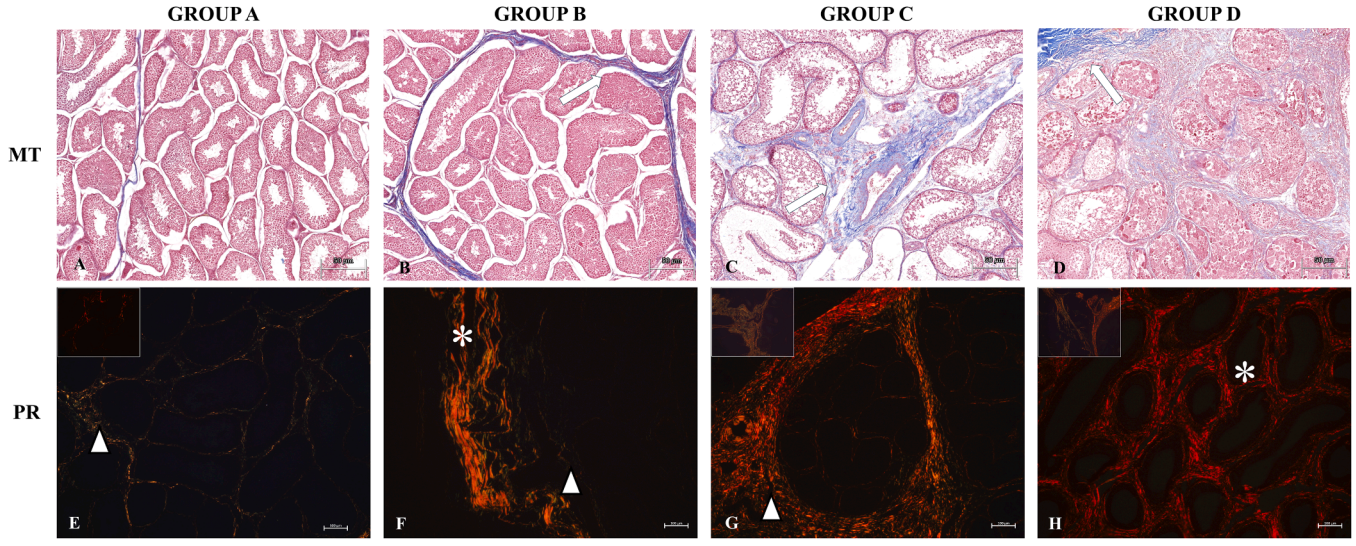

Fig. 5. Representative Masson's trichrome (A–D) and Picrosirius Red under polarised light (E–H) staining of testicular sections from Groups A–D. Masson's trichrome shows progressive interstitial collagen deposition from Group A to Group D, highlighted by white arrows in panels B–D. Picrosirius Red highlights red/orange birefringence (white arrowheads) and green/yellow-green birefringence (white asterisks). Insets in figures E, G, and H show additional representative areas from the same cases to illustrate the spatial heterogeneity of collagen birefringence. Original magnification, A–D, 40 × (scale bar = 50 μm); E–H, 20 × (scale bar = 100 μm).

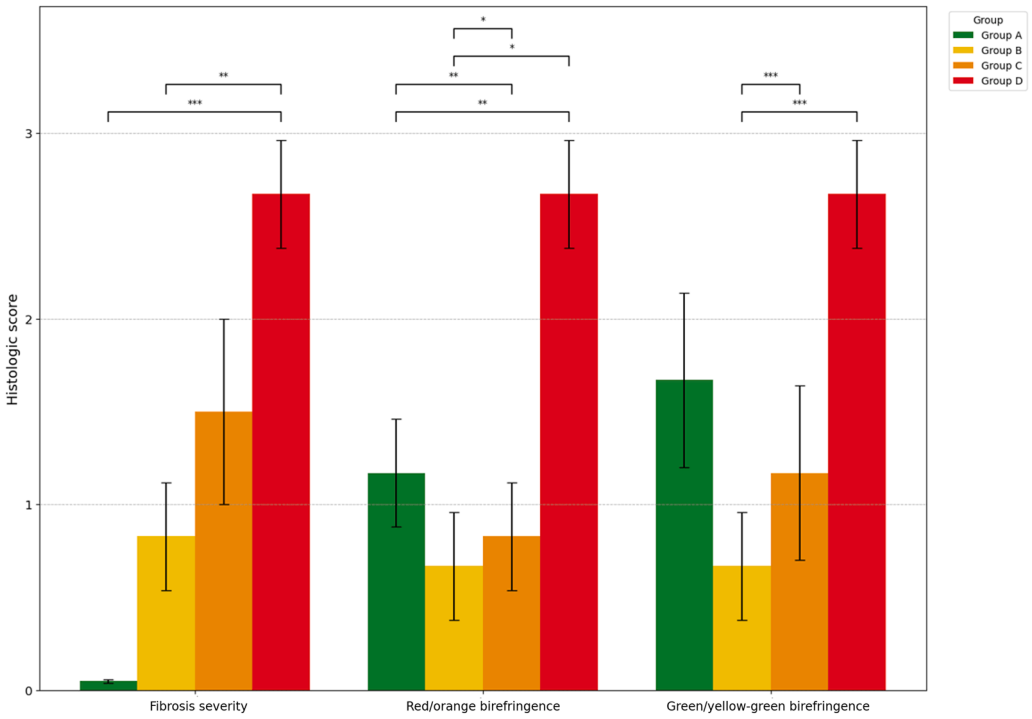

Fig. 6. Semi-quantitative analysis of interstitial fibrosis and collagen fibre birefringence patterns in testes from dogs with different spermatogenic status (Groups A–D). Bars indicate means ± SEM. Statistical significance was assessed using the Kruskal–Wallis test followed by Dunn's post hoc tests. Asterisks denote significant differences between groups (*p < 0.05; **p < 0.01; ***p < 0.001).

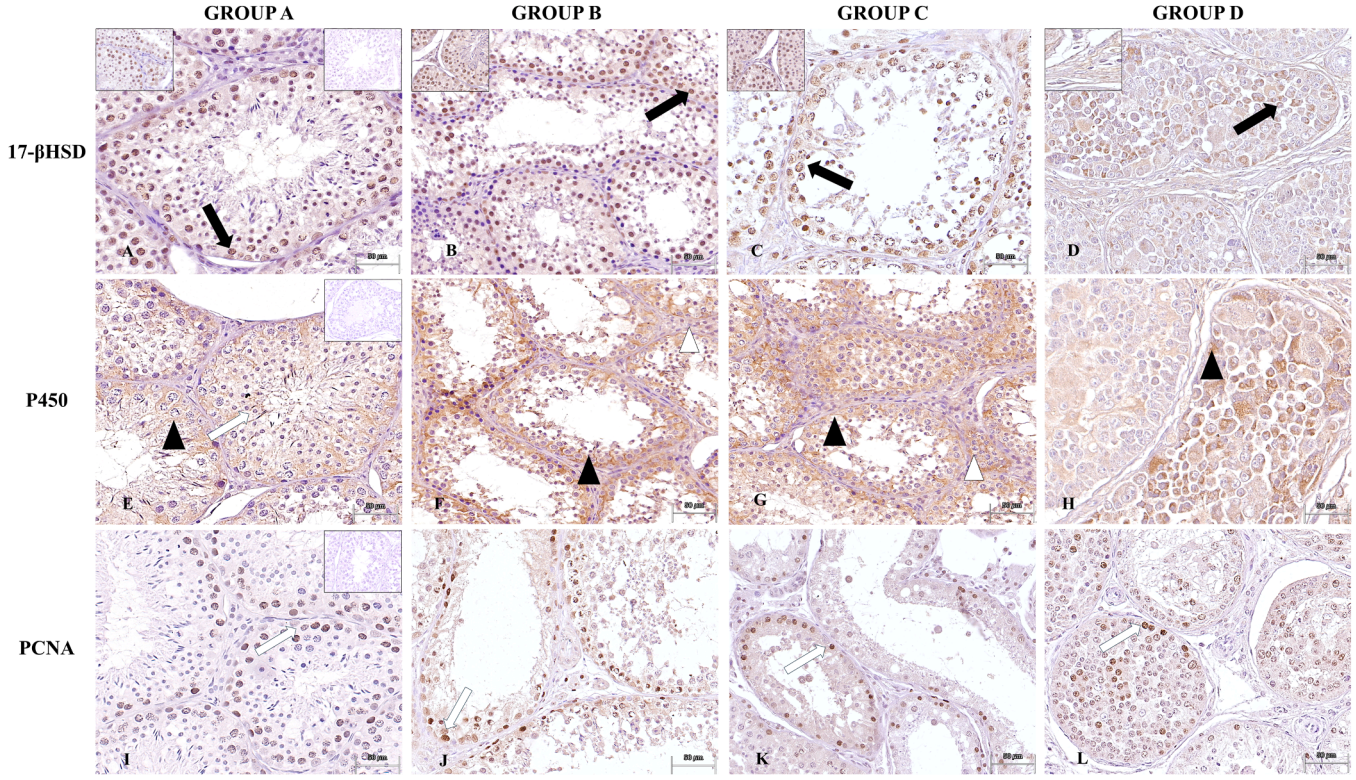

Fig. 7. Representative immunohistochemical staining for 17β-HSD (A–D), P450 aromatase (E–H), and PCNA (I–L) in testes from Groups A–D: Group A (A, E, I), Group B (B, F, J), Group C (C, G, K), and Group D (D, H, L). For 17β-HSD, both cytoplasmic and nuclear immunoreactivity are evident in spermatogonia (black arrows) and interstitial Leydig cells (top left insets) in Groups A–B, reduced in Group C, and present in neoplastic germ cells in Group D. P450 aromatase staining is observed in Sertoli cells (black arrowheads), spermatozoa (white arrow in E), and becomes more diffuse in pathological groups, including interstitial labelling (white arrowheads in F and G). PCNA highlights proliferating spermatogonia in non-neoplastic testes and numerous neoplastic germ cells in Group D (white arrows). Top right insets in panels A, E, and I show negative controls for 17β-HSD, P450 aromatase, and PCNA, respectively. Original magnification, 40 × ; scale bar = 20 μm.

PCNA immunoreactivity was exclusively nuclear. In Groups A–C, it was mainly detected in spermatogonia located in the basal compartment of the seminiferous tubules, whereas in Group D it was also evident in germ-cell/tumour-cell nuclei within neoplastic tubules. In Groups A and B, PCNA-positive nuclei were mainly observed in the basal compartment of the seminiferous tubules (Fig. 7I–J, white arrows). In Group C, nuclear immunoreactivity persisted in residual germ cells, although it was heterogeneously distributed in areas showing structural disorganization (Fig. 7K, white arrow). In neoplastic testes from Group D, a greater number of PCNA-positive germ-cell/tumour-cell nuclei was observed within neoplastic tubules (Fig. 7L, white arrow).

Negative controls for 17β-HSD, P450 aromatase, and PCNA showed no specific immunoreactivity (top right insets, Fig. 7A, E, and I, respectively). Immunoreactivity scores for 17β-HSD, cytochrome P450 aromatase, and PCNA across the four experimental groups are summarized in Table 3.

3.6. Western blot analyses

Semi-quantitative blot analysis showed that the bands corresponding to P450 aromatase (60 kDa), 17β-HSD (36 kDa), PCNA (36 kDa) and GAPDH (45 kDa) were detectable in all examined groups although with different intensity. Overall, Western Blot analysis showed an increase in aromatase levels and a decrease in 17β-HSD in pathological (Group C) and neoplastic cases (Group D) (Fig. 8A). In detail, P450 aromatase levels appeared normal in Groups A and B but increased in Groups C and D, with statistically significant differences (Group B vs Group C: $p < 0.001$; Group A vs Group D: $p < 0.05$) (Fig. 8B). Conversely, Groups A and B showed the highest levels of 17β-HSD compared to Groups C and D, where levels dramatically decreased, with significant differences (Group A vs Group B: $p < 0.05$; Group A vs Group C: $p < 0.01$; Group B vs Group D: $p < 0.05$) (Fig. 8B). Statistically significant differences were observed in PCNA expression between the assessed groups: Group B vs Group C: $p < 0.01$; Group C vs Group D: $p < 0.05$ (Fig. 8B). GAPDH bands were consistently detected in all groups and were used as internal loading control for normalization. After normalization to GAPDH, differences in target protein expression among groups remained statistically significant ($p < 0.05$).

4. Discussion

Over the last thirty years, growing concern has emerged in Campania Region regarding the health consequences of illegal waste dumping (Mazza et al., 2015; Comba et al., 2006). Environmental pollution represents a relevant issue for both human and animal health, as suggested by the parallel increase in infertility and tumour incidence reported in humans and dogs (Di Napoli et al., 2025; Chianese et al., 2026; Ottaiano et al., 2025; Spampinato et al., 2024; Triassi et al., 2015; Zaccaroni et al., 2014). Within this context, the present study found that testicular lesions were associated with higher concentrations of selected metals and metalloids. Chemical analysis identified the most robust group differences for Cd, Ni and U across both dog-level summarisation strategies, whereas Sn was retained only in the primary bilateral analysis and should therefore be interpreted cautiously. As, Cu, Mo and V showed only descriptive variation.

Table 3
Immunohistochemical scores across experimental groups.

Marker	Group A	Group B	Group C	Group D
17β-HSD	1.25 ± 0.04 (+)	1.17 ± 0.04 (+)	0.40 ± 0.04 (+)	0.70 ± 0.10 (+)
P450 aromatase	0.91 ± 0.04 (+)	1.10 ± 0.04 (+)	1.68 ± 0.06 (++)	1.61 ± 0.04 (++)
PCNA	0.90 ± 0.04 (+)	0.80 ± 0.04 (+)	1.13 ± 0.02 (+)	1.20 ± 0.04 (+)

In detail, the elevated levels of Cd are consistent with previous evidence showing that cadmium exposure can lead to spermatogenic toxicity and steroidogenic impairment (Wanjari and Gopalakrishnan, 2024; Zhu et al., 2020). Cadmium has been associated with blood–testis barrier disruption, oxidative stress, and dysfunction of Sertoli and Leydig cells, which may contribute to germ cell loss and steroidogenic imbalance (da Silva et al., 2021; De Angelis et al., 2017; Zhu et al., 2020). Therefore, our findings are in line with previous experimental evidence (Marinaro et al., 2024a, b; da Silva et al., 2021). In aquatic species, exposure to Cd has been demonstrated to cause morphological and structural alterations in the testis (Marinaro et al., 2024a), while, in murine models, Cd toxicity affecting spermatogenesis has been shown at several levels, including impairment of the blood-testis barrier and disruption of cell junctions (da Silva et al., 2021).

Moreover, chemical analysis highlighted that nickel showed significant differences across groups, largely due to its increase in neoplastic testes. This finding is toxicologically relevant because nickel exposure has also been associated with testicular structural damage, oxidative imbalance, and reproductive toxicity in experimental models, thus supporting its possible involvement in severe testicular injury within this cohort (Khlifi et al., 2013; Parveen et al., 2024).

Notably, all neoplastic testes showed higher Uranium levels, a finding of potential toxicological interest given previous evidence implicating uranium in testicular injury and carcinogenesis-related mechanisms (Joseph et al., 2021; Lu et al., 2021; Wang et al., 2020). Since uranium may enter biological systems through soil–water pathways and drinking water is considered a major route of intake (El-Taher, 2010; Wedepohl, 1995; Singh et al., 2008; World Health Organization, 2022), stray dogs may be particularly exposed because of scavenging behaviour and the use of uncontrolled water sources. Within a One Health framework, uranium bioaccumulation in dogs may therefore represent an early signal of environmental contamination relevant to human health, although our design does not allow inference on exposure sources or causality.

Overall, neoplastic testes exhibited markedly higher concentrations of Cd, Ni and U, with consistently large effect sizes in the comparisons between Group D and Groups A. These associations were confirmed in both the primary and the secondary sensitivity analysis (Cd: Cliff's $\delta = 0.65$; Ni: Cliff's $\delta = 0.80$–0.84; U: Cliff's $\delta = 0.70$–0.71). In this context, neoplastic tissue may show selective accumulation of some trace elements, potentially reflecting tumor-associated changes in vascular permeability, extracellular matrix remodelling, and cellular metal homeostasis (Lossow et al., 2021; Yaman et al., 2007; Kamiya, 2022; Pamphlett and Bishop, 2024). These findings should be interpreted as associations with the neoplastic state within this cohort, rather than evidence of a direct causal role in tumour development (Abdel-Gawad et al., 2016; Anđelković et al., 2023; Khlifi et al., 2013; Kuo et al., 2006; Soto-Heras et al., 2024; Strumylaitė et al., 2008; Nava-Castro et al., 2019). Another element showing bioaccumulation in testes with evident alterations was arsenic. This element is of clear toxicological relevance, as previous studies have linked its bioaccumulation to both testicular lesions and fibrogenic remodelling processes (Pant et al., 2001; Jana et al., 2006), suggesting a possible role in the mechanisms underlying structural damage to the testicular parenchyma. Copper and molybdenum, in turn, both tended to be higher in dogs with germ cell loss and more pronounced stromal remodelling. Although these differences did not remain statistically significant after correction for multiple testing, the finding is still biologically plausible: despite being essential trace elements, their excessive accumulation may disrupt delicate redox balance and interfere with testicular homeostasis (Kowal et al., 2010; Wang et al., 2016; Jiang et al., 2024; Zhao et al., 2024). Another measured element was vanadium. Although it showed only descriptive differences among groups, it may fit within this framework as a cofactor of multi-element exposure. From this perspective, the combined presence of copper, molybdenum, and vanadium may help define a more complex exposure profile, potentially associated with the most severe forms of

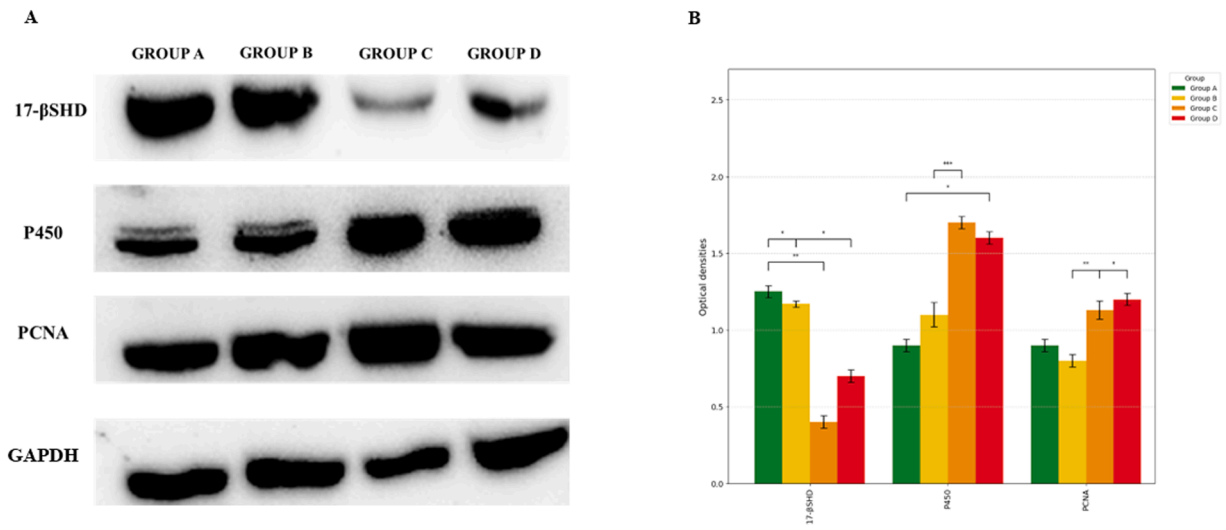

Fig. 8. Western blot analysis of 17β-HSD, P450 aromatase, and PCNA in testes from Groups A–D. (A) Representative blots. (B) Densitometric analysis normalised to GAPDH. Statistical significance was assessed using ANOVA followed by Tukey's post hoc test (*$p < 0.05$; **$p < 0.01$; ***$p < 0.001$). Data are expressed as mean ± SEM.

testicular injury (Llobet et al., 1993; Rodríguez-Lara et al., 2016). With regard to inorganic tin, current knowledge remains limited compared with the more extensively studied organotin compounds. Therefore, the Sn levels observed in this study should be interpreted with caution, without assigning any causal meaning, and rather considered as preliminary data supporting future investigations (Markmanuel et al., 2022).

Histological analysis also revealed more pronounced remodelling of the intertubular connective tissue in testes with higher concentrations of metals and metalloids, with a quantitative increase in collagen deposition and predominant red/orange birefringence under polarised light. Such birefringence patterns have traditionally been associated with differences in collagen fibre thickness and organisation, with green/yellow-green birefringence generally attributed to thinner, less organised fibres, and red/orange birefringence to thicker, more organised fibres (Junqueira et al., 1979; Lattouf et al., 2014). However, because these birefringence signals are also influenced by section thickness, fibre orientation, and imaging conditions (Dayan et al., 1989; López De Padilla et al., 2021), these patterns were treated in the present study as optical descriptors rather than as direct and unequivocal indicators of collagen maturation stage. The quantitative increase in collagen deposition, together with the predominance of red/orange birefringence in testes with higher metal and metalloid concentrations, may therefore be interpreted as a feature compatible with extracellular matrix remodelling and altered interstitial architecture (Serpe et al., 2012; Esposito et al., 2019; Lea et al., 2016).

Alongside these structural alterations, the mixed nuclear and cytoplasmic immunoreactivity observed for 17β-HSD warrants specific consideration. Although steroidogenic enzymes are generally associated with cytoplasmic or microsomal compartments, nuclear localisation has been reported for several members of the hydroxysteroid dehydrogenase family in different tissues and species (Dupont et al., 1991; Visus et al., 2011; Sivik et al., 2012; Muthusamy et al., 2011), suggesting that the subcellular distribution of these enzymes may vary depending on the isoform and tissue context. Since the subcellular localisation of HSD17B3 in canine testicular tissue has not been fully characterised, the nuclear component observed here was interpreted with caution, and the biological interpretation was based primarily on the cytoplasmic immunoreactivity within interstitial cells. Based on these findings, testes characterised by higher concentrations of metals and metalloids showed reduced expression of 17β-HSD and altered tissue distribution, accompanied by elevated levels of P450 aromatase, suggesting an imbalance in steroidogenic activity. These findings are consistent with endocrine-disrupting activity of these elements (Pocar et al., 2023; Sharpe, 2024) and with broader evidence indicating metals and metalloids may impair spermatogenesis (Kumar and Singh, 2022; López-Botella et al., 2021; Mukherjee et al., 2022; Sukhn et al., 2018). We further hypothesise that the progressive fibrotic remodelling of the interstitial compartment may contribute to an interstitial microenvironment unfavourable to Leydig cell function (Verderame et al., 2022). Because Leydig cells are a major source of 17β-HSD and testicular testosterone, their dysfunction may contribute to impaired spermatogenesis (Christin-Maitre and Young, 2022). This interpretation is consistent with the reduced PCNA expression observed in pathological groups, suggesting decreased spermatogonial proliferative activity and a reduced number of spermatogenic waves. Since these processes are androgen-dependent, the reduction in 17β-HSD may plausibly contribute to the altered spermatogenic patterns observed here (Christin-Maitre and Young, 2022). Conversely, increased aromatase expression is consistent with earlier evidence of a relationship between altered estrogen signaling and pathological/neoplastic phenotypes in the testis (Carreau and Hess, 2010; O'Donnell et al., 2001). PCNA expression was highest in neoplastic tissues, which is in accordance with the high proliferative activity, while the changes in non-neoplastic tissues may indicate compensatory or injury responses (Agnew and MacLachlan, 2016; Sumner et al., 2021). In summary, our findings indicate that dogs with severe degenerative/neoplastic phenotypes have a unique metallomic profile that is characterized by the simultaneous presence of multiple elements (De Falco and Laforgia, 2021; Mileo et al., 2023; Pocar et al., 2023; Zhu et al., 2023).

Consistently, the exploratory heatmap showed a relative enrichment of higher-burden profiles in Groups C and D. Because toxicological thresholds for canine testicular tissue are not available, the term "elevated" is used here only in reference to internal cohort-based comparisons. Published studies provide useful context, but not a direct benchmark, because they differ substantially in species, exposure setting, and analytical reporting criteria (Damek-Poprawa and Sawicka-Kapusta, 2003; Heidari et al., 2021; Ullah et al., 2023; Iyengar and Woittiez, 1988; Yang and Miyazaki, 2003). In conclusion, this preliminary intra-cohort study highlights that the bioaccumulation of specific metals in the testis is associated with the spermatogenic alterations observed. To the best of our knowledge, this is the first direct assessment of metals and metalloids in the canine testicular parenchyma within an exposed population. Although the study design does not allow

causal relationships to be established, the consistency of the associations observed between the analyzed elements and lesion severity supports the need for further investigations, particularly dose–response studies. In this context, the dog is confirmed as a particularly valuable model for the study of testicular alterations, providing a biologically relevant system for investigating the effects of environmental exposure on reproductive function.

5. Limitations

Although this preliminary study provides novel insights, a few limitations must be acknowledged. First, the study employs an intra-cohort design lacking a geographic control group from a non-polluted area, and direct environmental exposure metrics for individual dogs were unavailable. However, this design was specifically adopted to evaluate the internal correlation between tissue element burden and histopathological lesion severity within a documented high-risk environment. Second, stray dogs constitute a highly heterogeneous population regarding diet, baseline health status, and roaming behaviour. While this variability introduces potential confounding factors, it simultaneously represents a critical ecological strength: free-roaming dogs act as highly environmental sentinels. Finally, the absence of established reference background values and tissue-specific toxicological thresholds for canine testicular tissue limits the ability to define absolute 'normal' or 'toxic' levels. Consequently, our analytical interpretations were rigorously restricted to internal percentile variations. This limitation highlights the value of our dataset as a critical baseline for future environmental and reproductive toxicology studies in canine models.

6. Conclusions

This study represents the first intra-cohort evaluation of metals and metalloids in the testicular tissue of dogs from the Land of Fires. Within this cohort, both degenerative and neoplastic testicular lesions were associated with a distinct tissue elemental profile, suggesting that the distribution and bioaccumulation of specific elements may reflect different patterns of testicular injury. However, these findings do not establish a direct causal link between metal exposure and lesion development. Nevertheless, the integration of histological, molecular, and chemical data provides an integrated framework for future studies aimed to identify biomarkers of exposure and testicular damage in sentinel species, improving our understanding of the effects of environmental contaminants on reproductive health.

Funding

The authors received no specific funding for this work.

CRediT authorship contribution statement

Flavia Conte: Validation. **Claudia Cucolo:** Validation. **Marco Trifuoggi:** Resources. **Evaristo Di Napoli:** Visualization. **Angelo Spada:** Resources. **Nicola Ambrosio:** Resources. **Teresa Chianese:** Validation. **Maria De Falco:** Writing – review & editing. **Lorenzo Riccio:** Writing – review & editing, Writing – original draft, Visualization, Software, Methodology, Investigation, Formal analysis, Conceptualization. **Luigi Rosati:** Writing – review & editing, Supervision, Data curation, Conceptualization. **Orlando Paciello:** Writing – review & editing, Supervision, Funding acquisition.

Declaration of Competing Interest

The authors declare that they have no known competing financial interests or personal relationships that could have appeared to influence the work reported in this paper.

Acknowledgements

The authors thank Aleksey Costagliola for critical technical support in slide scanning and image digitization.

Appendix A. Supporting information

Supplementary data associated with this article can be found in the online version at doi:10.1016/j.etap.2026.105099.

Data availability

Data will be made available on request.

References

Abdel-Gawad, M., Elsobky, E., Shalaby, M.M., Abd-Elhameed, M., Abdel-Rahim, M., Ali-El-Dein, B., 2016. Quantitative evaluation of heavy metals and trace elements in the urinary bladder: Comparison between cancerous, adjacent non-cancerous and normal cadaveric tissue. Biol. Trace Elem. Res. 174 (2), 280–286.

Afzal, A., Mahreen, N., 2024. Emerging insights into the impacts of heavy metals exposure on health, reproductive and productive performance of livestock. Front. Pharmacol. 15, 1375137.

Agnese, M., Rosati, L., Coraggio, F., Valiante, S., Prisco, M., 2014. Molecular cloning of VIP and distribution of VIP/VPACR system in the testis of *Podarcis sicula*. Journal Experimental Zoology Part A Ecological Genetics Physiology 321, 334–347.

Agnew, D.W., MacLachlan, N.J., 2016. Tumors of the genital systems. Tumors Domest. Anim. 689–722.

Alberti, P., 2022. The 'land of fires': epidemiological research and public health policy during the waste crisis in Campania, Italy. Heliyon 8 (12).

Anđelković, M., Djordjevic, A.B., Vukelić, D., Đukić-Ćosić, D., Aćimović, M., Bojanić, N., Bulat, Z., 2023. Cadmium and lead implication in testis cancer; Is there a connection? Chemosphere 330, 138698.

Bencze, J., Szarka, M., Kóti, B., Seo, W., Hortobágyi, T.G., Bencs, V., Hortobágyi, T., 2021. Comparison of semi-quantitative scoring and artificial intelligence aided digital image analysis of chromogenic immunohistochemistry. Biomolecules 12 (1), 19.

Carreau, S., Hess, R.A., 2010. Oestrogens and spermatogenesis. Philos. Trans. R. Soc. B Biol. Sci. 365 (1546), 1517–1535.

CASRN, 2007. Method. 6020a inductively Couple Plasma-Mass. Spectrom.

Chen, X., Cao, S., Wen, D., Zhang, Y., Wang, B., Duan, X., 2023. Domestic dogs as sentinels of children lead exposure: Multi-pathway identification and source apportionment based on isotope technique. Chemosphere 316, 137787.

Chianese, T., Trinchese, G., Leandri, R., De Falco, M., Mollica, M.P., Scudiero, R., Rosati, L., 2024. Glyphosate exposure induces cytotoxicity, mitochondrial dysfunction and activation of ERα and ERβ estrogen receptors in human prostate PNT1A cells. Int. J. Mol. Sci. 25, 7039.

Chianese, T., Galati, M., Cappello, T., Maisano, M., Lettieri, G., Marinaro, C., Piscopo, M., Fasciolo, G., Gravato, C., Napolitano, G., Paolella, G., Locascio, A., Scudiero, R., Rosati, L., 2026. Exploring the Impact of Polystyrene Microplastic Beads on Male Gonads of the Marine Mussel, *Mytilus galloprovincialis*. Environ. Toxicol. 41 (7), 379–394. https://doi.org/10.1002/tox.24581.

Christin-Maitre, S., Young, J., 2022. Androgens and spermatogenesis. Ann. D. 'Endocrinol. 83 (3), 155–158.

Comba, P., Bianchi, F., Fazzo, L., Martina, L., Menegozzo, M., Minichilli, F., Mitis, F., Musmeci, L., Pizzuti, R., Santoro, M., Trinca, S., Martuzzi, M., "Health Impact of Waste Management Campania" Working Group, 2006. Cancer mortality in an area of Campania (Italy) characterized by multiple toxic dumping sites. Ann. New. Y. Acad. Sci. 1076, 449–461.

d'Aquino, I., Piegari, G., Miletti, G., Sannino, E., Costanza, D., Meomartino, L., Paciello, O., 2023. Morphometrical and immunohistochemical evaluation of kidney as an indirect parameter to estimate age in puppies in veterinary forensic pathology. Animals 13, 2665.

d'Aquino, I., Riccio, L., Piegari, G., Ambrosio, N., Longobardi, C., Ciarcia, R., Cortese, L., Di Napoli, E., Paciello, O., Russo, V., 2026. Association between urinary cotinine and whole-slide digital cytomorphometric alterations in the oral mucosa of tobacco smoke-exposed cats. Vet. Sci. 13 (4), 354. https://doi.org/10.3390/vetsci13040354.

da Silva, J., Goncalves, R.V., de Melo, F.C.S.A., Sarandy, M.M., da Matta, S.L.P., 2021. Cadmium exposure and testis susceptibility: A systematic review in murine models. Biol. Trace Elem. Res. 199 (7), 2663–2676.

Damek-Poprawa, M., Sawicka-Kapusta, K., 2003. Damage to the liver, kidney, and testis with reference to burden of heavy metals in yellow-necked mice from areas around steelworks and zinc smelters in Poland. Toxicology 186 (1–2), 1–10.

Damiano, S., Longobardi, C., Ferrara, G., Piscopo, N., Riccio, L., Russo, V., Ciarcia, R., 2023. Oxidative status and histological evaluation of wild boars' tissues positive for zearalenone contamination in the Campania region, southern Italy. Antioxidants 12 (9), 1748.

Dayan, D., Hiss, Y., Hirshberg, A., Bubis, J.J., Wolman, M., 1989. Are the polarization colors of picrosirius red-stained collagen determined only by the diameter of the fibers? Histochemistry 93 (1), 27–29.

De Angelis, C., Galdiero, M., Pivonello, C., Salzano, C., Gianfrilli, D., Piscitelli, P., Pivonello, R., 2017. The environment and male reproduction: The effect of cadmium exposure on reproductive function and its implication in fertility. Reprod. Toxicol. 73, 105–127.
De Falco, M., Laforgia, V., 2021. Combined effects of different endocrine-disrupting chemicals (EDCs) on prostate gland. Int. J. Environ. Res. Public. Health 18, 9772.
Di Napoli, E., De Biase, D., Degli Uberti, B., Dimatteo, M., Baldi, L., Cavallo, S., Paciello, O., 2025. Testicular Tumors and Environmental Pollution: A Comparative Oncoepidemiology Study in the Campania Region from 2020 to 2023. Vet. Sci. 12 (8), 695.
Dupont, E.R.I.C., Labrie, F., Luu-The, V., Pelletier, G., 1991. Localization of 17 beta-hydroxysteroid dehydrogenase throughout gestation in human placenta. J. Histochem. & Cytochem. 39 (10), 1403–1407.
El-Taher, A., 2010. INAA and DNAA for uranium determination in geological samples from Egypt. Appl. Radiat. Isot. 68 (6), 1189–1192.
Esposito, M., De Roma, A., Maglio, P., Sansone, D., Picazio, G., Bianco, R., Gallo, P., 2019. Heavy metals in organs of stray dogs and cats from the city of Naples and its surroundings (Southern Italy). Environ. Sci. Pollut. Res. 26 (4), 3473–3478.
Ferrante, M.C., Di Vaio, P., Magli, E., Frecentese, F., Meli, R., Caliendo, G., Perissutti, E., 2020. PCB levels in adipose tissue of dogs from illegal dumping sites in Campania region (Italy). Chemosphere 244, 125478.
Fuller, R., Landrigan, P.J., Balakrishnan, K., Bathan, G., Bose-O'Reilly, S., Brauer, M., Yan, C., 2022. Pollution and health: a progress update. Lancet Planet. Health 6 (6), e535–e547.
Grison, S., Legendre, A., Svilar, L., Elie, C., Kereselidze, D., Gloaguen, C., Souidi, M., 2022. Multigenerational exposure to uranium changes sperm metabolome in rats. Int. J. Mol. Sci. 23 (15), 8349.
Hampton, J.O., Cobb, M.L., Toop, S.D., Flesch, J.S., Hyndman, T.H., 2023. Elevated lead exposure in Australian hunting dogs during a deer hunting season. Environ. Pollut. 323, 121317.
Heidari, A.H., Zamiri, M.J., Nazem, M.N., Shirazi, M.R.J., Akhlaghi, A., Pirsaraei, Z.A., 2021. Detrimental effects of long-term exposure to heavy metals on histology, size and trace elements of testes and sperm parameters in Kermani sheep. Ecotoxicol. Environ. Saf. 207, 111563.
Hmidi, I., Riccio, L., Chianese, T., Knani, L., Rosati, L., Hmida, L., 2026. Gonadic cycle and environmental modulation of P450 aromatase localization in Cerastoderma glaucum ovary from Monastir Bay. Comp. Biochem. Physiol. A: Mol. Integr. Physiol. 313, 111966.
Iyengar, V., Woittiez, J., 1988. Trace elements in human clinical specimens: Evaluation of literature data to identify reference values. Clin. Chem. 34 (3), 474–481.
Jana, K., Jana, S., Samanta, P.K., 2006. Effects of chronic exposure to sodium arsenite on hypothalamo-pituitary-testicular activities in adult rats: Possible an estrogenic mode of action. Reprod. Biol. Endocrinol. 4 (1), 9.
Jiang, L., Yang, F., Liao, H., Chen, W., Dai, X., Peng, C., Cao, H., 2024. Molybdenum and cadmium cause blood-testis barrier dysfunction through ROS-mediated NLRP3 inflammasome activation in sheep. Sci. Total. Environ. 906, 167267.
Johnsen, S.G., 1970. Testicular biopsy score count–A method for registration of spermatogenesis in human testes: Normal values and results in 335 hypogonadal males. Horm. Res. Paediatr. 1 (1), 2–25.
Joseph, S.J., Arunachalam, K.D., Murthy, P.B., Ramalingam, R., Musthafa, M.S., 2021. Uranium induces genomic instability and slows cell cycle progression in human lymphocytes in acute toxicity study. Toxicol. Vitr. 73, 105149.
Junqueira, L.C.U., Bignolas, G., Brentani, R.R., 1979. Picrosirius staining plus polarization microscopy, a specific method for collagen detection in tissue sections. Histochem. J. 11 (4), 447–455.
Kamiya, T., 2022. Copper in the tumor microenvironment and tumor metastasis. J. Clin. Biochem. Nutr. 71 (1), 22–27.
Khlifi, R., Olmedo, P., Gil, F., Hammami, B., Chakroun, A., Rebai, A., Hamza-Chaffai, A., 2013. Arsenic, cadmium, chromium and nickel in cancerous and healthy tissues from patients with head and neck cancer. Sci. Total. Environ. 452, 58–67.
Kowal, M., Lenartowicz, M., Pecio, A., Gołas, A., Błaszkiewicz, T., Styrna, J., 2010. Copper metabolism disorders affect testes structure and gamete quality in male mice. Syst. Biol. Reprod. Med. 56 (6), 431–444.
Kumar, N., Singh, A.K., 2022. Impact of environmental factors on human semen quality and male fertility: A narrative review. Environ. Sci. Eur. 34, 6.
Kuo, C.Y., Wong, R.H., Lin, J.Y., Lai, J.C., Lee, H., 2006. Accumulation of chromium and nickel metals in lung tumors from lung cancer patients in Taiwan. J. Toxicol. Environ. Health Part. A 69 (14), 1337–1344.
López De Padilla, C.M., Coenen, M.J., Tovar, A., De la Vega, R.E., Evans, C.H., Müller, S. A., 2021. Picrosirius red staining: revisiting its application to the qualitative and quantitative assessment of collagen type I and type III in tendon. J. Histochem. & Cytochem. 69 (10), 633–643.
López-Botella, A., Velasco, I., Acién, M., Sáez-Espinosa, P., Todolí-Torró, J.L., Sánchez-Romero, R., Gómez-Torres, M.J., 2021. Impact of heavy metals on human male fertility—An overview. Antioxidants 10 (9), 1473.
Lattouf, R., Younes, R., Lutomski, D., Naaman, N., Godeau, G., Senni, K., Changotade, S., 2014. Picrosirius red staining: a useful tool to appraise collagen networks in normal and pathological tissues. J. Histochem. & Cytochem. 62 (10), 751–758.
Lea, R.G., Byers, A.S., Sumner, R.N., Rhind, S.M., Zhang, Z., Freeman, S.L., England, G.C. W., 2016. Environmental chemicals impact dog semen quality in vitro and may be associated with a temporal decline in sperm motility and increased cryptorchidism. Sci. Rep. 6, 31281.
Legendre, A., Gloaguen, C., Kereselidze, D., Saci, N., El Houdigui, S.M., Froment, P., Grison, S., 2025. Multigenerational effects of uranium exposure reveal stronger testicular dysregulation in the second generation. Curr. Res. Toxicol., 100279
Llobet, J.M., Colomina, M.T., Sirvent, J.J., Doningo, J.L., Corbella, J., 1993. Reproductive toxicity evaluation of vanadium in male mice. Toxicology 80 (2–3), 199–206.
Lossow, K., Schwarz, M., Kipp, A.P., 2021. Are trace element concentrations suitable biomarkers for the diagnosis of cancer? Redox Biol. 42, 101900.
Lovaković, B.T., 2020. Cadmium, arsenic, and lead: Elements affecting male reproductive health. Curr. Opin. Toxicol. 19, 7–14.
Lu, B., Ran, Y., Wang, S., Li, J., Zhao, Y., Ran, X., Hao, Y., 2021. Chronic oral depleted uranium leads to reproductive damage in male rats through the ROS-hnRNP A2/B1-COX-2 signaling pathway. Toxicology 449, 152666.
Marinaro, C., Marino, A., Bianchi, A.R., Berman, B., Trifuoggi, M., Marano, A., Palumbo, G., Chianese, T., Scudiero, R., Rosati, L., De Maio, A., Lettieri, G., Piscopo, M., 2024b. Molecular and toxicological mechanisms behind the effects of chromium (VI) on the male reproductive system of *Mytilus galloprovincialis*: First evidence for poly-ADP-ribosylation of protamine-like II. ISSN 0009-2797 Chem. -Biol. Interact. 401 (2024), 111186. https://doi.org/10.1016/j.cbi.2024.111186.
Marinaro, C., Lettieri, G., Chianese, T., Bianchi, A.R., Zarrelli, A., Palatucci, D., Piscopo, M., 2024a. Exploring the molecular and toxicological mechanism associated with interactions between heavy metals and the reproductive system of *Mytilus galloprovincialis*. Comparative Biochemistry Physiology Part C Toxicology & Pharmacology 275, 109778.
Markmanuel, D.P., Amos-Tautau, B.M.W., Songca, S.P., 2022. Tin concentrations and human health risk assessment for children and adults in seafood and canned fish commonly consumed in Bayelsa State, Nigeria. J. Appl. Sci. Environ. Manag. 26 (7), 1263–1269.
Mazza, A., Piscitelli, P., Neglia, C., Rosa, G.D., Iannuzzi, L., 2015. Illegal dumping of toxic waste and its effect on human health in Campania, Italy. Int. J. Environ. Res. Public. Health 12, 6818–6831.
Mileo, A., Chianese, T., Fasciolo, G., Venditti, P., Capaldo, A., Rosati, L., De Falco, M., 2023. Effects of dibutylphthalate and steroid hormone mixture on human prostate cells. Int. J. Mol. Sci. 24, 14341.
Mukherjee, A.G., Wanjari, U.R., Renu, K., Vellingiri, B., Gopalakrishnan, A.V., 2022. Heavy metal and metalloid-induced reproductive toxicity. Environ. Toxicol. Pharmacol. 92, 103859.
Muthusamy, S., Andersson, S., Kim, H.J., Butler, R., Waage, L., Bergerheim, U., Gustafsson, J.Å., 2011. Estrogen receptor β and 17β-hydroxysteroid dehydrogenase type 6, a growth regulatory pathway that is lost in prostate cancer. Proc. Natl. Acad. Sci. 108 (50), 20090–20094.
Nava-Castro, K.E., Ramírez-Nieto, R., Méndez-García, L.A., Girón-Pérez, M.I., Segovia-Mendoza, M., Navidad-Murrieta, M.S., Morales-Montor, J., 2019. Environmental pollution as a risk factor in testicular tumour development: Focus on the interaction between bisphenol A and the associated immune response. Int. J. Environ. Res. Public. Health 16, 4113.
O'Donnell, L., Robertson, K.M., Jones, M.E., Simpson, E.R., 2001. Estrogen and spermatogenesis. Endocr. Rev. 22 (3), 289–318.
Ottaiano, M., Baldi, L., Del Monaco, V., Brunetti, R., Pellicanò, R., Cavallo, S., De Carlo, E., 2025. Incidence rates of tumors in dogs in southern Italy—Focus on the Campania region—2018/2022. Ital. J. Food Saf. 14 (4).
Pamphlett, R., Bishop, D.P., 2024. Elemental biomapping of human tissues suggests toxic metals such as mercury play a role in the pathogenesis of cancer. Front. Oncol. 14, 1420451.
Pant, N., Kumar, R., Murthy, R.C., Srivastava, S.P., 2001. Male reproductive effect of arsenic in mice. Biometals 14, 113–117.
Parveen, S., Rizvi, A., Akhtar, K., Khan, A.A., Naseem, I., 2024. Nickel-induced oxidative stress causes cell death in testicles: Implications for male infertility. Naunyn-Schmiede 'S. Arch. Pharmacol. 397 (3), 1659–1670.
Piegari, G., d'Aquino, I., Salanti, G.V., Romano, V., Miletti, G., Sannino, E., Paciello, O., 2024. Pathological changes and sodium rhodizonate test as tools for investigating gunshot wounds in veterinary forensic pathology. Animals 14 (19), 2913.
Pocar, P., Grieco, V., Aidos, L., Borromeo, V., 2023. Endocrine-disrupting chemicals and their effects in pet dogs and cats: An overview. Animals 13, 378.
Power, K., Riccio, L., Siciliano, A., Santorufo, L., Rosati, L., Landi, S., Maisto, G., 2026. Impact of conventional vs. biodegradable and compostable microplastics on *Eisenia fetida* S.: An ecopathological approach. Environ. Toxicol.
Prüss-Üstün, A., Wolf, J., Corvalán, C., Bos, R., Neira, M., 2016. Preventing disease through healthy environments: a global assessment of the burden of disease from environmental risks. World Health Organization.
Remeteiová, D., Ružičková, S., Mičková, V., Laubertová, M., Slezáková, R., 2020. Evaluation of US EPA method 3052 microwave acid digestion for quantification of majority metals in waste printed circuit boards. Metals 10 (11), 1511.
Riccio, L., Chianese, T., Mileo, A., Balsamo, S., Sciarrillo, R., Gatta, R., Capaldo, A., 2025. Changes of CB1 receptor expression in tissues of cocaine-exposed eels. Animals 15, 1734.
Rodríguez-Lara, V., Morales-Rivero, A., Rivera-Cambas, A.M., Fortoul, T.I., 2016. Vanadium inhalation induces actin changes in mice testicular cells. Toxicol. Ind. Health 32 (2), 367–374.
Rosati, L., Chianese, T., De Gregorio, V., Verderame, M., Raggio, A., Motta, C.M., Scudiero, R., 2023. Glyphosate interference in follicular organization in the wall lizard *Podarcis siculus*. Int. J. Mol. Sci. 24, 7363.
Serpe, F.P., Russo, R., De Simone, A., Florio, S., Esposito, M., Severino, L., 2012. Levels of heavy metals in liver and kidney of dogs from urban environment. Open. Vet. J. 2 (1), 15–18.
Sharpe, R.M., 2024. Endocrine disruption and male reproductive disorders: unanswered questions. Human. Reprod. 39 (9), 1879–1888.
Singh, J., Singh, H., Singh, S., Bajwa, B.S., 2008. Estimation of uranium and radon concentration in some drinking water samples. Radiat. Meas. 43, S523–S526.

Sivik, T., Vikingsson, S., Gréen, H., Jansson, A., 2012. Expression patterns of 17β-hydroxysteroid dehydrogenase 14 in human tissues. Horm. Metab. Res. 44 (13), 949–956.

Soto-Heras, S., Reinacher, L., Wang, B., Oh, J.E., Bunnell, M., Park, C.J., Ko, C.J., 2024. Cryptorchidism and testicular cancer in the dog: Unresolved questions and challenges in translating insights from human studies. Biol. Reprod. 111, 269–291.

Spampinato, M., Siciliano, A., Travaglione, A., Chianese, T., Mileo, A., Libralato, G., Guida, M., Trifuoggi, M., De Gregorio, V., Rosati, L., 2024. Unravelling the ecotoxicological impacts of gadolinium (Gd) on *Mytilus galloprovincialis* embryos and sperm in seawater: A preliminary study, 17 Heliyon 10 (10), e31087. https://doi.org/10.1016/j.heliyon.2024.e31087.

Strumylaitė, L., Boguševičius, A., Ryselis, S., Pranys, D., Poškienė, L., Kregždytė, R., Asadauskaitė, R., 2008. Association between cadmium and breast cancer. Medicina 44 (6), 415.

Sukhn, C., Awwad, J., Ghantous, A., Zaatari, G., 2018. Associations of semen quality with non-essential heavy metals in blood and seminal fluid: Data from the Environment and Male Infertility (EMI) study in Lebanon. J. Assist. Reprod. Genet. 35 (9), 1691–1701.

Sumner, R.N., Harris, I.T., Van der Mescht, M., Byers, A., England, G.C.W., Lea, R.G., 2020. The dog as a sentinel species for environmental effects on human fertility. Reproduction 159, R265–R276.

Sumner, R.N., Byers, A., Zhang, Z., Agerholm, J.S., Lindh, L., England, G.C., Lea, R.G., 2021. Environmental chemicals in dog testes reflect their geographical source and may be associated with altered pathology. Sci. Rep. 11, 7361.

Triassi, M., Alfano, R., Illario, M., Nardone, A., Caporale, O., Montuori, P., 2015. Environmental pollution from illegal waste disposal and health effects: A review on the "Triangle of Death". Int. J. Environ. Res. Public. Health 12 (2), 1216–1236.

Ullah, S., Ennab, W., Wei, Q., Wang, C., Quddus, A., Mustafa, S., Shi, F., 2023. Impact of cadmium and lead exposure on camel testicular function: Environmental contamination and reproductive health. Animals 13 (14), 2302.

Vaccaro, E., Navas, L., Ercolano, M., Piegari, G., Di Napoli, E., Papparella, S., Russo, V., 2024. Immunohistochemical Investigation of Cyclooxygenase-2 Expression in Rabbit Uterine Adenocarcinoma and the Potential Use of COX-2 Inhibitors in Cancer Therapy. Animals 14 (22), 3169.

Verderame, M., Chianese, T., Rosati, L., Scudiero, R., 2022. Molecular and histological effects of glyphosate on testicular tissue of the lizard *Podarcis siculus*. Int. J. Mol. Sci. 23, 4850.

Vinnikov, D., Syurin, S., 2024. Nickel and human sperm quality: A systematic review. BMC Public. Health 24 (1), 3545.

Visus, C., Ito, D., Dhir, R., Szczepanski, M.J., Chang, Y.J., Latimer, J.J., DeLeo, A.B., 2011. Identification of Hydroxysteroid (17β) dehydrogenase type 12 (HSD17B12) as a CD8+ T-cell-defined human tumor antigen of human carcinomas. Cancer Immunol. Immunother. 60 (7), 919–929.

Wang, H.W., Zhou, B.H., Zhang, S., Guo, H.W., Zhang, J.L., Zhao, J., Tian, E.J., 2016. Reproductive toxicity in male mice after exposure to high molybdenum and low copper concentrations. Toxicol. Ind. Health 32, 1598–1606.

Wang, S., Ran, Y., Lu, B., Li, J., Kuang, H., Gong, L., Hao, Y., 2020. A review of uranium-induced reproductive toxicity. Biol. Trace Elem. Res. 196 (1), 204–213.

Wanjari, U.R., Gopalakrishnan, A.V., 2024. Cadmium as a male reproductive toxicant and natural and non-natural ways to tackle it: A review. Environ. Sci. Pollut. Res. 31, 18340–18361.

Wedepohl, K.H., 1995. The composition of the continental crust. Geochim. Et. Cosmochim. Acta 59, 1217–1232.

World Health Organization, 2022. Guidelines for drinking-water quality: incorporating the first and second addenda. World Health Organization.

Yaman, M., Kaya, G., Yekeler, H., 2007. Distribution of trace metal concentrations in paired cancerous and non-cancerous human stomach tissues. World J. Gastroenterol. 13 (4), 612.

Yang, J., Miyazaki, N., 2003. Moisture content in Dall's porpoise (*Phocoenoides dallī*) tissues: A reference base for conversion factors between dry and wet weight trace element concentrations in cetaceans. Environ. Pollut. 121 (3), 345–347.

Zaccaroni, A., Corteggio, A., Altamura, G., Silvi, M., Di Vaia, R., Formigaro, C., Borzacchiello, G., 2014. Elements levels in dogs from "triangle of death" and different areas of Campania region (Italy). Chemosphere 108, 62–69.

Zappulli, V., Moccia, V., Torrigiani, F., Molinari, A., Detillo, P., Gola, C., Bussolati, B., 2026. Non-toxic acid-free glyoxal fixative for veterinary gross specimen preservation, histopathology, immunohistochemistry, and molecular analysis. Vet. Pathol. 63 (2), 282–295.

Zhao, D., Wu, L., Fang, X., Wang, L., Liu, Q., Jiang, P., Han, H., 2024. Copper exposure induces inflammation and PANoptosis through the TLR4/NF-κB signaling pathway, leading to testicular damage and impaired spermatogenesis in Wilson disease. Chem. -Biol. Interact. 396, 111060.

Zhu, L., Hajeb, P., Fauser, P., Vorkamp, K., 2023. Endocrine disrupting chemicals in indoor dust: A review of temporal and spatial trends, and human exposure. Sci. Total. Environ. 874, 162374.

Zhu, Q., Li, X., Ge, R.S., 2020. Toxicological effects of cadmium on mammalian testis. Front. Genet. 11, 527.